Transition of cavitating flow to supercavitation within Venturi nozzle – hysteresis investigation

Kozák Jiří[1,*], *Rudolf* Pavel[1], *Huzlík* Rostislav[2], *Hudec* Martin[1], *Chovanec* Radomír[1], *Urban* Ondřej[1], *Maršálek* Blahoslav[3], *Maršálková* Eliška[3], *Pochylý* František[1] and *Štefan* David[4]

[1]Brno University of Technology, FME, Victor Kaplan Dept. of Fluid Engineering, Brno, Czech Republic
[2]Brno University of Technology, FEEC, Dept. of Power Electrical and Electronic Engineering, Brno, Czech Republic
[3]The Czech Academy of Sciences, Centre for Cyanobacteria and Their Toxins, Brno, Czech Republic
[4]Laval University, Department of Mechanical Engineering, Québec, Canada

Abstract. Cavitation is usually considered as undesirable phenomena. On the other hand, it can be utilized in many applications. One of the technical applications is using cavitation in water treatment, where hydrodynamic cavitation seems to be effective way how to reduce cyanobacteria within large bulks of water. The main scope of this paper is investigation of the cavitation within Venturi nozzle during the transition from fully developed cavitation to supercavitation regime and vice versa. Dynamics of cavitation was investigated using experimental data of pressure pulsations and analysis of high speed videos, where FFT of the pixel intensity and Proper Orthogonal Decomposition (POD) of the records were done to identify dominant frequencies connected with the presence of cavitation. The methodology of the high speed (HS) records semi-automated analysis using the FFT was described. Obtained results were correlated and above that the possible presence of hysteresis was discussed.

1 Introduction

Cavitation plays a crucial role in design process as well as operation of many hydraulic machines such as turbines, pumps and valves. Despite the fact that occurrence of this phenomenon is usually considered as an undesirable condition, it is possible to utilize its concomitants in many positive ways.

Among the most significant side effects of cavitation belongs occurrence of pressure pulsations and erosion of the surfaces exposed to the cavitation bubbles implosions. These conditions lead to the reduction of the hydraulic machines efficiency, lifespan and operation range (Dörfler [1]).

On the other hand, the same effects of cavitation can be utilized for example in medical industry, chemical industry, cleaning and water treatment.

The main scope of this contribution is study of the transition between cavitation and supercavitation regime of flow within the axisymmetric Venturi tube, where the pressure drop in the constriction leads to inception of cavitation. This device can be exploited for the efficient reduction of the cyanobacteria bloom in large bulks of water (Jančura et al [2]). This contribution complements the previously presented papers, which were focused on the wider range of cavitation regimes. [3],[4]

Comprehensive study of cavitation and its detection within Venturi nozzle can be found in [5].

During the experimental research, the severe pressure pulsation as well as increase of the overall noise were observed prior the transition to the supercavitation regime of the flow. In addition, the correct evaluation of the experimental transition between fully developed cavitation and supercavitation has been considerably challenging compared to the other regimes with higher cavitation numbers.

These reasons led to decision to devote particular attention to the research of the transition using several methods of the experimental data evaluation. Especially methods of the high-speed video records postprocessing using the POD of the chosen region of interest and FFT of the pixel intensity fluctuations.

During the previous research utilizing the FFT of the pixel intensity, it became evident that the proper choice of the source pixel is the trickier, the lower is the cavitation number. Thus the evaluation of these regimes was usually excluded to prevent potentially misleading results. For these purpose, the automated choice of the source pixel based on root mean square of the pixel intensity within the chosen region was utilized. Results of all of the previously mentioned methods were compared and correlated. The software for the HS records analysis has been coded using the Python and OpenCV library.

Above the aforementioned verification of these methodologies of the cavitation dynamics evaluation, the hypothesis of the potential hysteresis during the transition caused by the residual cavitation nuclei has been done. Hysteresis during the investigation was examined from the hydraulic losses point of view as well as frequency of

* Corresponding author: jiri.kozak1@gmail.com

instabilities connected with the presence and motion of the cavitating structures.

2 Experimental set-up and Venturi nozzle geometry description

The experimental measurement has been carried out using the cavitation rig of the Victor Kaplan's Dept. of fluid engineering. The rig was equipped by the transducers recording the pressure upstream and downstream the Venturi nozzle, discharge within the system and temperature of the water in the reservoir.

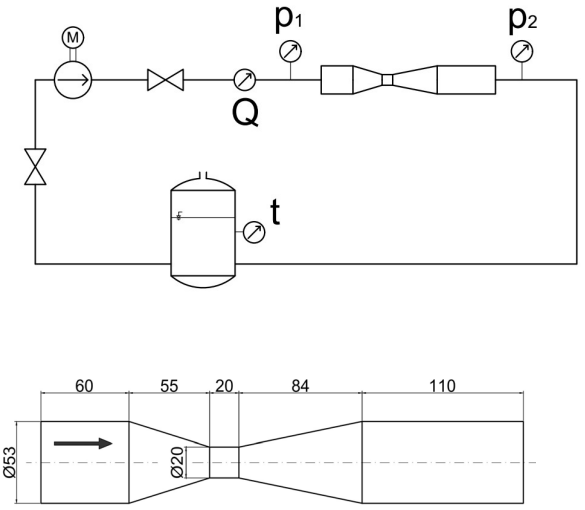

Fig. 1. Scheme of the cavitation rig and Venturi nozzle

Reservoir has been opened to the atmosphere, thus the cavitation number has been altered only by the change of the discharge. The experimental measurement has been carried out repeatedly. It should be noted that the presence of the cavitation nuclei has not been measured during the experiments. Water within the cavitation rig was deaerated by the operation in the supercavitation regime for 30 minutes prior the measurement. The list of the utilized transducers can be found in the Table 1

Table 1. List of transducers (Note: Acc – accuracy in % of the measured value* or % of the transducer measuring range**).

Variable	Manufacturer	Type	Acc.
p_1	BD SENSORS	DMP 331	± 0,25%*
p_2	BD SENSORS	DMP 331	± 0,25%*
Q	ELA Brno	MQI99-SN	±0,5%*
t	HIT Uherské Hradiště	HSO-502 1A2L	±0,1%**

HS Photron FastcamSA-X2 1000K has been utilized during the measurement A. Grayscale records with the sampling frequency of 20 000 fps and resolution of 1024x512 pixels captures 0.5 s of the cavitating flow have been captured.
Unfortunately, during this measurement the critical failure of the thermometer occurred, thus the saturated vapor pressure as well as water density was considered constant using the water temperature of 20°C.
Increase of the temperature has been captured during the measurement B, but without the connection with HS video records. This measurement has been carried out twice to partially prove reproducibility of the results (B_1 and B_2).

3 Computation of the water properties

The water properties necessary for the proper evaluation were computed using the recorded values of the temperature, discharge and pressures.
Density of the water ρ was computed as a function of the water temperature using the following formula:

$$\rho = 1002 - 0.2716t + 0.01047t^2 - 0.00027t^3 \quad (1)$$

Value of saturated vapour pressure was computed using the exponential function of the thermodynamic temperature. [6]

$$p_{vap} = \frac{e^{77.3450 + 0.0057\,T - \frac{7235}{T}}}{T^{8.2}} \quad (2)$$

Using computed values of the water density, saturated vapor pressure and measured values of the pressure downstream the nozzle, the value of cavitation number can be expressed using the eq.3.

$$\sigma = \frac{p_2 - p_{vap}}{0.5\,\rho {v_{th}}^2} \quad (3)$$

Where v_{th} represents the velocity of the flow within the constriction of the Venturi tube.
Hydraulic loss coefficient of the Venturi tube was computed and evaluated using the equation (4) in the whole range of the investigated cavitation regimes

$$\xi = \frac{p_1 - p_2}{0.5\,\rho {v_{th}}^2} \quad (4)$$

4 Methodology of the high speed records post processing

Various operating points have been investigated during the measurement A in order to capture transition between cavitation and supercavitation and vice versa. Two different methods of the HS records analysis have been introduced and their result have been correlated with the spectral analysis of the pressure fluctuations downstream the nozzle. The basic description of these methods is the content of the following sections.
It should be mentioned that although the sampling frequency of the camera and pressure transducers were different, the start of the data recording was synchronized using a voltage signal ramp.

4.1 FFT analysis of the pixel intensity fluctuations

Description of the theoretical and mathematical background of this method of the signal spectral analysis exceeds scope of this contribution, nevertheless it can be found in the literature. [7]
The source of the data for the spectral analysis is represented by the fluctuations of the pixel intensity which vary from 0 to 255 in case of grayscale HS video. The presence of interfacial interphase leads to a reflection of the light and therefore increases brightness of the region affected by the cavitation. Comparison of the HS video analysis with pressure fluctuations can be found in [8], where cavitation over NACA profile was investigated or in [4] where analysis of C-D nozzle was presented.
While in case of the initial phases of cavitation (e.g. higher values of the σ) the proper choice of the source pixel does not pose the problem, it became problematic with the fully developed stage of cavitation and its transition to the supercavitation. These regimes are distinguished by the significant amount of cavitation within the flow, which complicates proper illumination of the region of interest. It is usually not possible to supress occurrence of the over- and underexposed regions during recording of the cavitation. The improper choice of the pixel intensity can be source of the misleading results.
Manual choice of the proper source pixel can be time consuming and above that it can be misleading due to the introduction of human factor.
Thus the semi-automated method of the source pixel choice has been utilized. Larger region of interest was configured manually to prevent regions with significant presence of over exposed pixels and capturing characteristic fluctuations of the cavitation at the same time. The source pixel has been automatically selected from this region based on the largest intensity fluctuations root mean square value RMS_{int} within the region. (eq. 5)

$$RMS_{int} = \sqrt[2]{\frac{1}{N}\sum_{i=1}^{N}\left(I_i - I_{avg}\right)^2} \tag{5}$$

Where: N represents the number of samples of the record, I_i is the greyscale intensity of the pixel in the sample and I_{avg} represents the average intensity of the pixel computed using the whole length of record.

4.2 Proper Orthogonal Decomposition of the High speed records

POD represents an effective way how to decompose a complex physical phenomenon into the several POD modes while it can be assumed that the most of the information related to the dominant instability is contained in the first several POD modes. In other words, the most significant flow structures within the investigated flow can be relatively easily identified.
Although the fact that this method can be utilized for the analysis of the vector quantities and provide deeper insight in the physical nature of the phenomenon, the utilization of POD is limited to the processing of the scalar pixel intensity of the HS records in this contribution. Due to this fact, the brief description of this method will be limited to the analysis of scalar quantities.
Exhaustive description of this method can be found in [9]. Using the variant of POD called method of snapshot, the time dependent eigenfunctions $\boldsymbol{a_i}$ and spatio-dependent functions $\boldsymbol{\phi_i}$ are computed in order to find an approximation of a general spatio-temporal dependent variable $\boldsymbol{u}(\boldsymbol{x};\boldsymbol{t})$ (in this case pixel intensity I) within the domain Ω. For this purpose, the correlation matrix $\boldsymbol{C_{ij}}$ is constructed using the samples of the record with known sampling frequency according to the next equation.

$$\boldsymbol{C_{ij}} = \frac{1}{vol\Omega}\int_{\Omega} \mathrm{u}(\mathbf{x};\,\mathrm{t}_i)\,\mathrm{u}(\mathbf{x};\,\mathrm{t}_j)\mathrm{d}\mathbf{x} \tag{6}$$

Solving the eigenvalue problem of the correlation matrix $\boldsymbol{C_{ij}}$, the eigenvalues and eigenvectors are obtained. Considering that the eigenvalue λ is paired with corresponding eigenvector $\boldsymbol{e}$ and the fact that value of λ is directly connected with contribution of the corresponding POD mode, the eigenvalues and eigenvectors are sorted by the magnitude of the eigenvalues. Temporal coefficients a_i and spatial eigenmodes $\boldsymbol{\phi_i}$ are then computed using the following expressions:

$$\boldsymbol{a_i} = \boldsymbol{e_i}\sqrt{N\lambda_i} \tag{7}$$

$$\boldsymbol{\phi_i} = \boldsymbol{U}\frac{\boldsymbol{e_i}}{\sqrt{N\lambda_i}} \tag{8}$$

Where N is the number of the samples and $\boldsymbol{U}$ is matrix consisting of all recorded samples transformed to the form of column vectors (matrix of size M by N size where M is the number of pixels within one sample and N is the number of the recorded samples).
Dominant frequency of the selected mode i can be then evaluated by the spectral analysis of the correspondent temporal coefficient a_i.
Several applications of POD for the cavitating flow dynamics investigation can be found in the literature. Comprehensive study of the cavitating spiral vortex within the elbow draft tube was done by Štefan et al [10]. The POD analysis of the HS video capturing cavitation cloud over NACA profile was done by Rudolf et al [11].
Influence of the aeration on the cavitation patterns downstream within the Venturi tube was the scope of investigation which has been done by Tomov et al [12]. The operation regimes in this study corresponded to the partially developed stage of cavitation.
POD study of the cavitation regime detection in case of grooved C-D nozzle was done by Danlos et al [13].

5 Experimental measurement

As it was mentioned above, the presented contribution is focused on the cavitation regimes corresponding the transition from the fully developed cavitation to the supercavitation. Results of the two experimental sets focused on transition between fully developed cavitation and vice versa are described in the following chapters.

5.1 Experimental measurement A

During the first set of experimental measurements the HS camera has been utilized. Unfortunately, the temperature and its increase during the first part of experiments has not been captured. On the other hand, based on the measurement B, the growth of the water temperature should not exceed 1°C during the whole cycle of measurements (e.g from cavitation to supercavitation and back to the initial operating point). Thus the constant temperature 20°C has been considered. This approach neglects the change of water density as well as the change of the saturated vapor pressure and viscosity. Above that the potential nonlinearity of the temperature growth during the measured cycle has not been captured.
On the other hand, thanks to the known maxim magnitude of the temperature growth and the fact that the main scope of this part of measurement has been to correlate several methods of the cavitation dynamics investigation, the water temperature differences can be neglected.

5.1.1 Cavitation patterns during the transition

Cavitation numbers σ varied from the value of 0.27 corresponding to the supercavitation to 0.34 of the fully developed cavitation prior to the transition.
It should be noted that the behaviour of the cavitating flow was almost independent on the direction of the flowrate change. The only noticed difference was an amount of the small bubbles, which was slightly higher in case of increasing discharge (in the cavitation → supercavitation direction). It should be emphasized that this observation is only subjective.
The cycle of fully developed cavitation stage within Venturi tube starts with the inception near the throat edges (Figure 2).

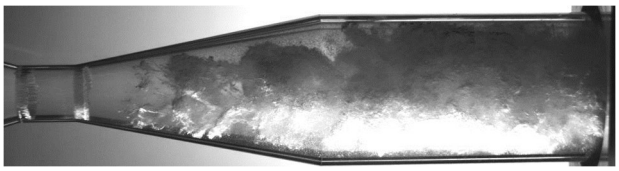

Fig. 2. Start of the new cavitation cycle. (Q = 7.76 l/s, σ = 0.33)

The amount of observable cavitation grows in the diffuser downstream the throat and its partial separation is well observable at the certain moment (Figure 3).

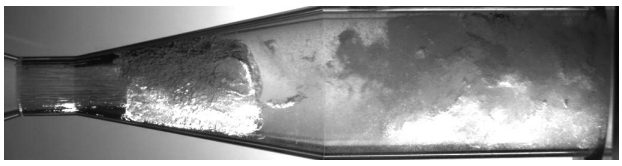

Fig. 3. Growth of the cavitation cloud within the diffuser (Q = 7.76 l/s, σ = 0.33)

The cavitation cloud is entrained by the flow downstream the nozzle, while the frontal part of cavitation collapses towards the throat (Figure 4).

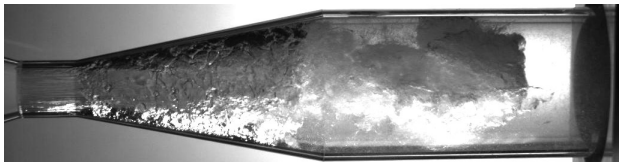

Fig. 4. Partial separation of the cavitation cloud (Q = 7.76 l/s, σ = 0.33)

Collapse of the cavitating cloud is accompanied by the creation of the significant amount of instabilities near the axis and cavitating vortices in the nozzle (Figure 5).

Fig. 5. Visible instabilities near the axis of the Venturi tube (Q = 7.76 l/s, σ = 0.33)

The cavitation near the throat disappears completely and new cycle starts prior the decay of the cavitating cloud downstream the nozzle (Figure 6).

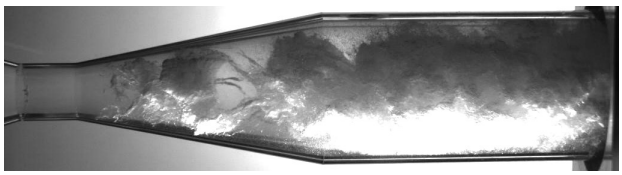

Fig. 6. Complete decay of the cavitation within the constriction of the tube right prior the beginning of new cycle (Q = 7.76 l/s, σ = 0.33)

With the increasing discharge the instabilities near the axis became more coherent and occasionally start to form stabilized jet in the axis of the nozzle which is depicted in the Figure 7. Jet became the more dominant the lower is cavitation number. Above that cavitation cloud became more massive and its partial separation became less visible.

Fig. 7. Visible jet during the transition between cavitation regimes (Q = 8.34 l/s, σ = 0.29)

With the transition to the pure supercavitation regime (Figure 8), the noise as well as the pressure pulsations induced by the fluctuations of cavitation became significantly lower.
The jet near the axis of the nozzle is stable most of the time and collapses with very low frequency.

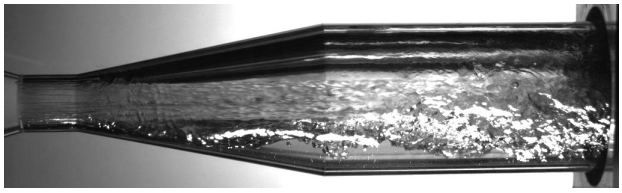

Fig. 8. Coherent jet visible during the supercavitation (Q = 8.56 l/s, σ = 0.27)

5.1.2 *Spectral analysis of the pixel intensity fluctuations*

The matrix of size 20 by 20 pixels has been chosen as the region, where the source pixel was selected based on the value of root mean square of the intensity fluctuations. Position of the source matrix in the diffuser downstream the constriction is in the Figure 9.

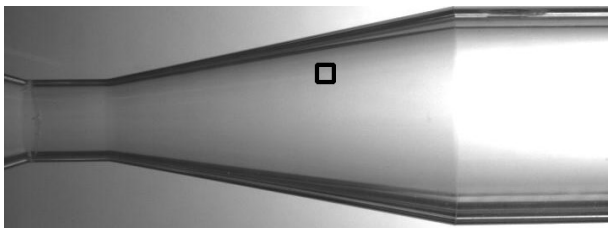

Fig. 9. Position of source matrix within the diffuser

It is clearly depicted that the RMS image of the pixel matrix is the more homogenous the higher cavitation number is (Figure 10).

Fig. 10. RMS image of the source matrix in case of increasing Q. Fully developed cavitation: Q = 7.67 l/s, σ = 0.34; Transition Q = 8.34 l/s, σ = 0.29 and supercavitation Q = 8.55 l/s, σ = 0.27 (Note: Red – high intensity RMS, Blue – low intensity RMS)

While the value of intensity RMS within the matrix is nearly constant in case of fully developed cavitation, the proper choice of the pixel became more important in case of supercavitation, where the distribution of the intensity RMS value became rather uneven.
Results of pixel intensity fluctuations FFT analysis are depicted in the Figure 11. It should be emphasized that the results were not adjusted or filtered. Depicted dominant frequencies were obtained automatically based on the maximum value of the pulsations amplitudes without any further adjustment.
It is clearly depicted that the dominant frequencies are decreasing with decreasing cavitation numbers in whole spectrum of the investigated operating points. The only exception can be found in case of increasing discharge (in the chart marked by the red cross). Values of the pixel intensity fluctuations frequency are decreasing from approximately 50 Hz, which corresponds to the pulsations of the cavitation in case of fully developed cavitation to 2 Hz in case of supercavitation.
There is no significant difference between the results acquired for decreasing and increasing discharge. Therefore, a possible occurrence of the cavitation hysteresis cannot be confirmed using FFT analysis of the pixel intensity fluctuations. Results of the spectral analysis will be correlated with the results of other methods in one of the following chapters.

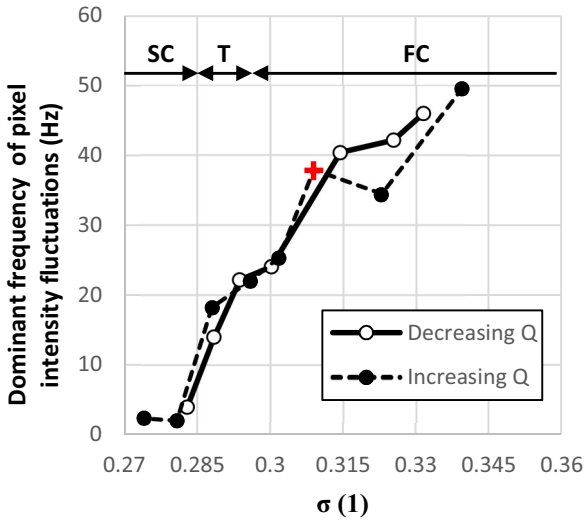

Fig. 11. Dominant frequencies of the pixel intensity fluctuations (S – supercavitation, T – transition, FC – fully dev. cavitation.)

5.1.3 *POD analysis of the HS records*

Region of interest (ROI) has been chosen for the purpose of the POD analysis as is depicted in the Figure 12. Position and size of the ROI was set-up so that typical patterns of cavitation were captured in whole spectrum of investigated cavitation numbers, while presence of the overexposed regions was minimized.

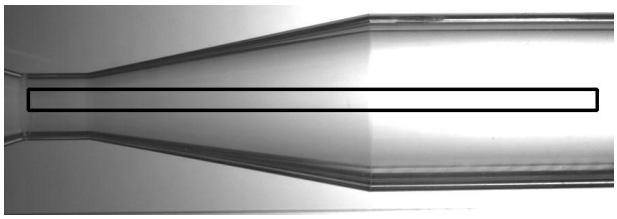

Fig. 12. Region of interest for the POD analysis

It should be noted that unlike the FFT of pixel intensity fluctuations, where all of the available samples were considered for the purpose of analysis, in case of POD only each tenth sample has been utilized in the decomposition. Skipping of the samples was motivated mainly by the reducing of the computational demands, considering fact, that lowered sampling frequency will be still more than sufficient for the purpose of the presented analysis. The POD analysis has been carried out using the values of pixel intensity fluctuations, e.g. the average image was obtained in the first step of analysis and then distracted from the record sample by sample.

Results of the POD were analysed then. The comparison of the relative as well as cumulative contribution of the POD modes is depicted in the following charts.
It is clearly depicted that the overall tendencies are similar regardless the direction of discharge change. The lower is cavitation number, the lower significance of the most dominant POD modes is. In other words, with decreasing cavitation number more information about the captured flow is stored in less significant modes.
For the purpose of the results comparison the threshold value of 80% of cumulative significance has been chosen. While the threshold value is reached summing less than 50 POD modes in case of fully developed cavitation, more than 200 modes are needed for the same result in case of transition between cavitation and supercavitation. (Fig. 13 and 14)

Obtained results suggest, that the supercavitation regime of the flow has occurred earlier in case of the increasing discharge. Curve of the POD modes cumulative significance is considerably closer to the curve depicting supercavitation in case of the transition regime (Fig. 14) compared to the results of decreasing discharge (Fig. 13). Direct comparison of the results is shown in the Figure 15.
On the other hand, the correct evaluation of the results during the transition can be challenging and this conclusion will be verified in the following text using another experimental method. It should be also verified by the analysis of longer records. Larger amount of POD modes needed to reach 80% of cumulative significance also agree with the observation of slightly higher amount of small bubbles in case of records capturing cavitation during the cycle of increasing discharge.

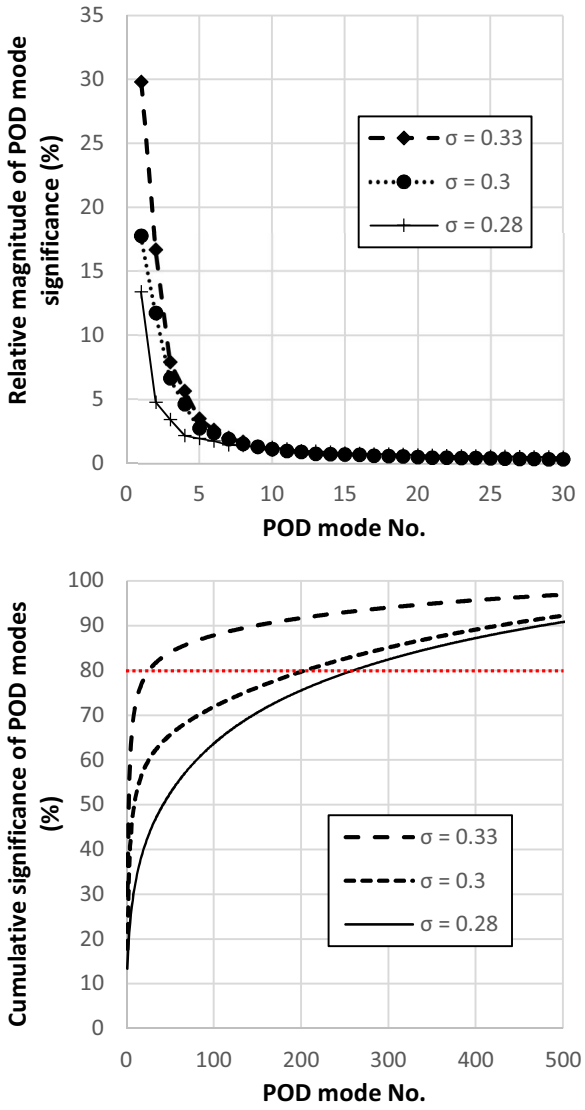

Fig. 13. Charts depicting relative and cumulative contributions of the POD modes significance in case of decreasing discharge.

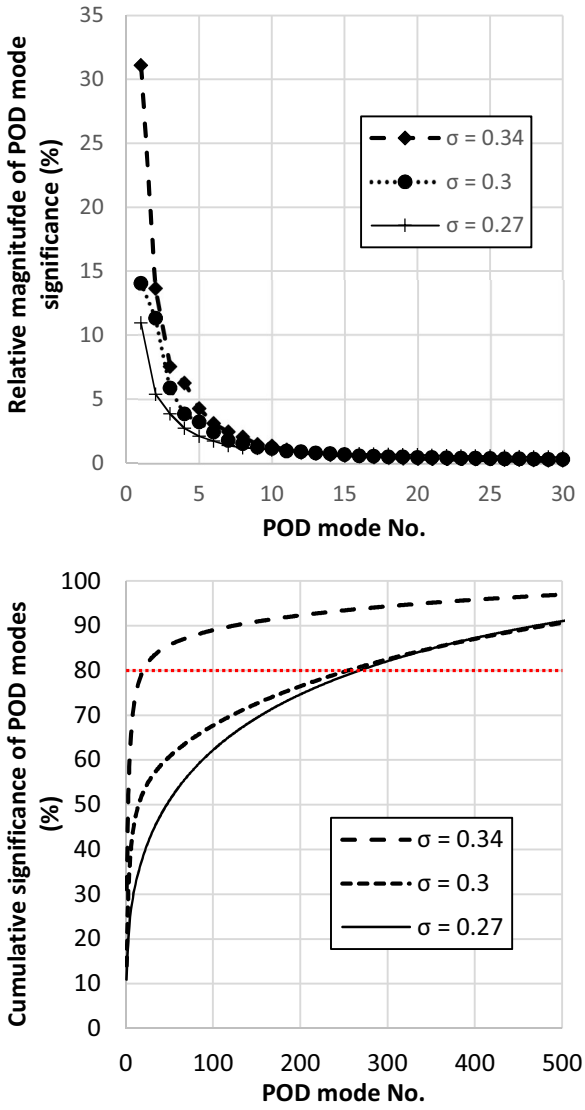

Fig. 14. Charts depicting relative and cumulative contributions of the POD modes significance in case of increasing discharge.

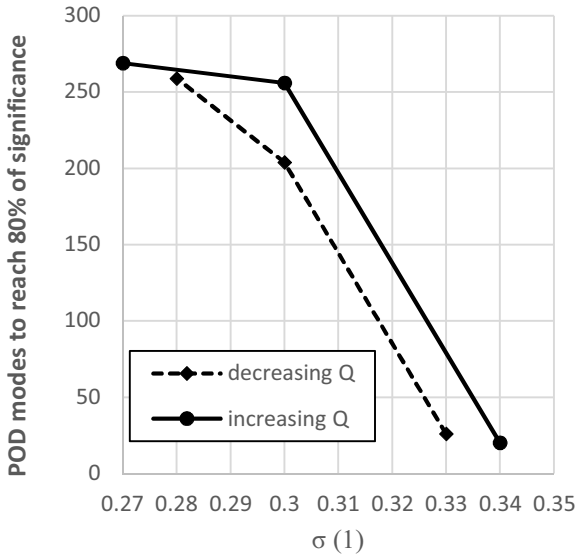

Fig. 15. Number of POD modes needed to reach 80% of cumulative significance.

Dynamics of the most significant POD modes has been investigated using FFT analysis of the corresponding time dependent eigenfunctions a_i. Ten most significant modes have been analyzed and the dominant frequencies were determined based on this analysis.

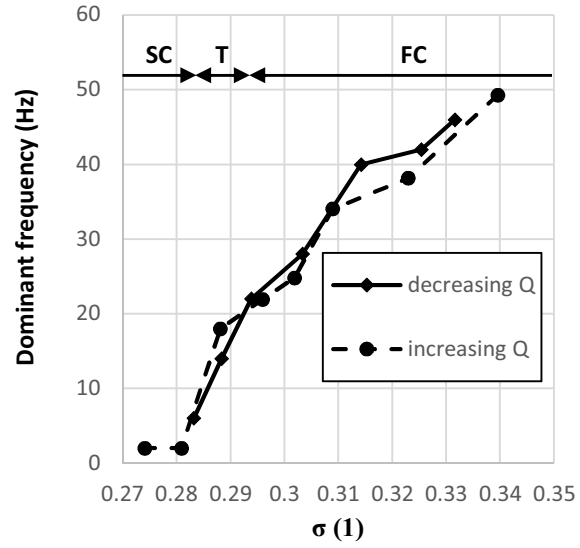

Fig. 16. Spectral analysis of the time-dependent eigenfunctions corresponding to the most significant POD modes.

Results of the spectral analysis depict decreasing frequency of dominant instabilities with the decreasing cavitation number similar to the results of pixel intensity fluctuations FFT analysis. Dominant frequencies corresponding to the increasing discharge are slightly lower compared to the decreasing Q in the region of fully developed cavitation. (Figure 16)
This result corresponds to the larger amount of bubbles which have been observed during the experiments. Small bubbles can act as an additional source of dampening, which decreases frequency of pulsations.
To complete the description of the POD, the most significant spatial eigenmode ϕ_0 of selected operating point as well as the corresponding fluctuations (*a_fluct*) of time dependent eigenfunction a_0 and its spectral analysis are depicted in the Figure 17.

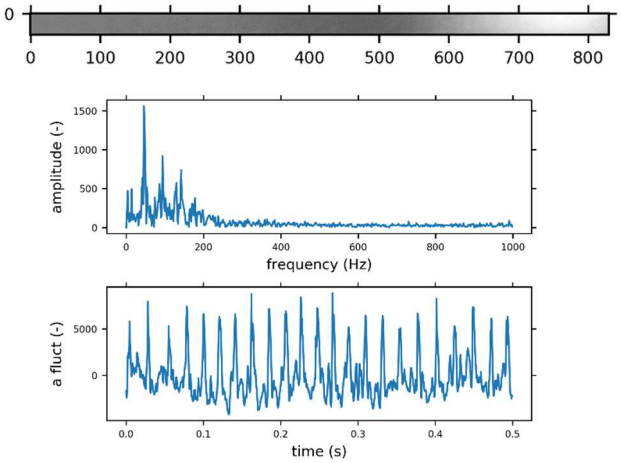

Fig. 17. The most dominant spatial eigenmode (scale in px) with corresponding time dependent eigenmode and its spectral analysis (Q = 7.76 l/s, σ = 0.33)

Compared to the most significant POD mode the spatial eigenmode corresponding to the 10th most significant POD mode is considerably less homogenous and frequency spectra of its time dependent eigenfunction is significantly noisier (Figure 18). This observation refers to the fact, that the less significant POD modes capture smaller instabilities within the recorded cavitating flow.

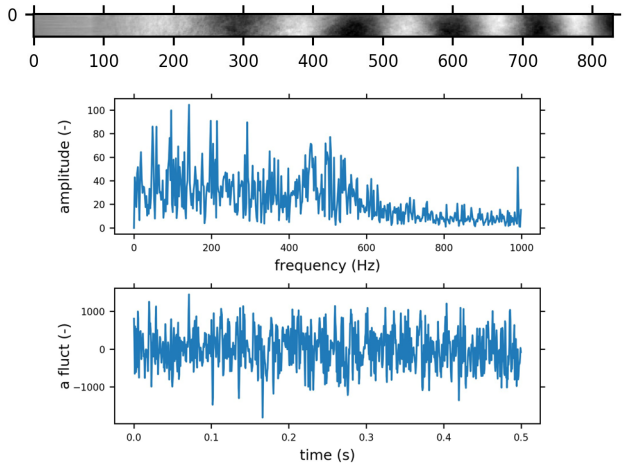

Fig. 18. 10th most significant spatial eigenmode (scale in px) with corresponding time dependent eigenmode and its spectral analysis (Q = 7.76 l/s, σ = 0.33)

5.1.4 Spectral analysis of pressure fluctuations and final correlation of results

Pressure fluctuations downstream the Venturi nozzle have been recorded and analysed to provide benchmark results. It should be emphasized, that the investigation of the cavitation dynamics using the pressure analysis can be more challenging compared to the analysis of the image data in case of lower cavitation number values. This became particularly evident in case of supercavitation when the pressure transducer is located in region of

saturated vapour. The results of the pressure fluctuations analysis are depicted in the following Figure 19.

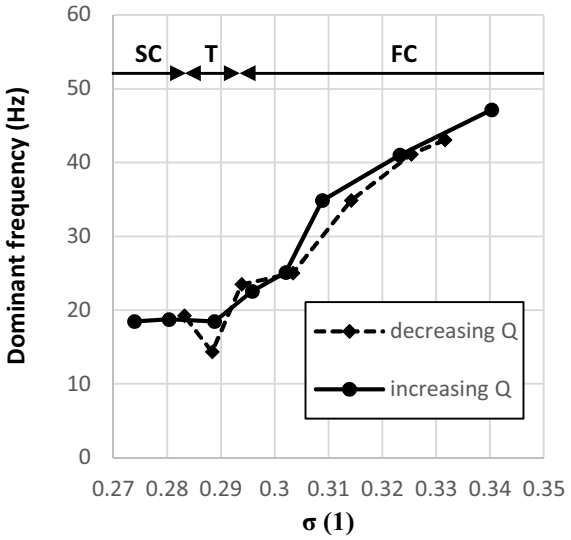

Fig. 19. Spectral analysis of pressure fluctuations downstream the nozzle

Decreasing values of dominant frequencies with the decreasing values of cavitation number have been captured again, similar to the analysis of the HS records. The values of dominant frequencies were slightly lower in case increasing discharge in the region of fully developed cavitation.

Correlation of the utilized methods is depicted in the following figures. Figure 20 is depicting results of increasing discharge. It is obvious that the dominant frequencies evaluated using the pressure fluctuations are considerably higher compared to the results of both methods of HS video analysis in case of supercavitation.

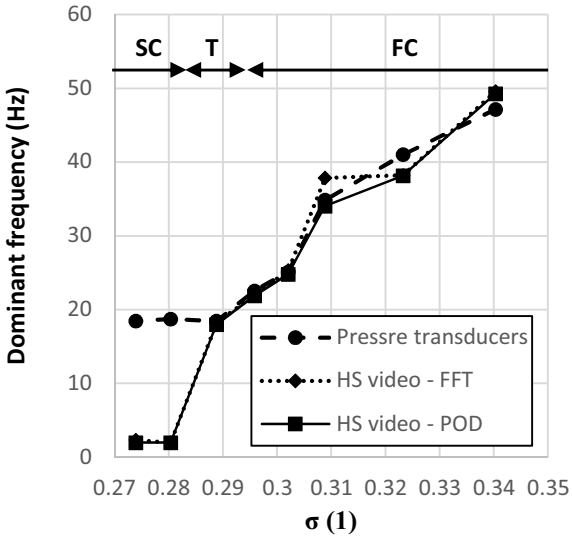

Fig. 20. Correlation of the methods of cavitation dynamics investigation – increasing discharge

Slightly different are the results of correlation in case of decreasing discharge (Figure 21). The more significant difference of image analysis methods compared each other can be found in the region of supercavitation.

Quite interesting is the fact that the results are in good agreement in case of transition between regimes.

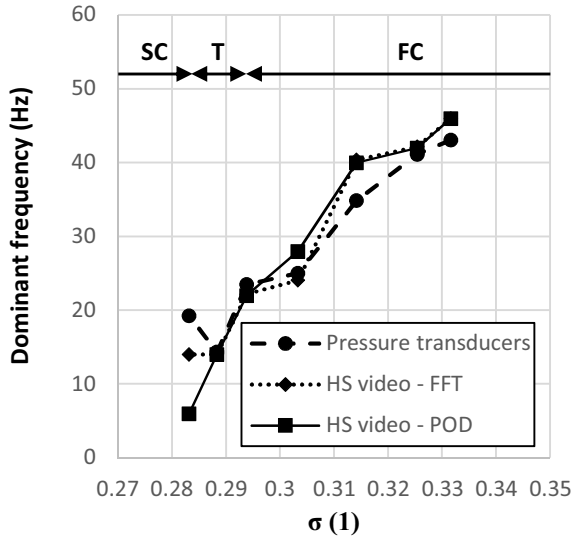

Fig. 21. Correlation of the methods of cavitation dynamics investigation – decreasing discharge

Based on the previous results it can be stated that the utilized methods of the cavitation dynamics analysis are fully comparable in case of higher cavitation numbers (fully developed cavitation and transition).

It should be noted that the frequencies captured by FFT of pressure fluctuations in case of supercavitation can be found as one of the significant frequencies in case of POD. Therefore, it is possible to assume that the most dominant source of pressure fluctuation is not identical to the most dominant source of image instability in case of supercavitation.

5.2 Experimental measurement B

Temperature of the water was not recorded during the measurement A. This led to the neglecting of the change of saturated vapor pressure as well as density of the water during the experiments as it was mentioned.

To capture the influence of the water properties change, the second measurement (B) has been carried out. Beside the measurement of temperature, the position of pressure transducers has been modified to provide undistorted data for the purpose of the hydraulic losses evaluation.

The measurement B has been done repeatedly to partially prove reproducibility of the results (B1 and B2).

The results of the pressure fluctuations spectral analyses of both of the measurement are depicted in the following figures (22 and 23).

Overall tendencies of the obtained dominant frequencies are similar to the measurement A. It should be noted that one of the operating point was excluded in case of measurement B1 considering increasing discharge (black cross in the Figure 22). Dominant frequency was significantly higher compared to the close neighborhood of the this operating point.

The transition between cavitation regimes started earlier in case of increasing Q. This behavior has been observed in both of the measurements B1 and B2 (Figure 22 and 23). On the other hand, the results suggest that the transition between regimes is more abrupt in case of the decreasing discharge and fully developed supercavitation can be observed prior to the increasing discharge.

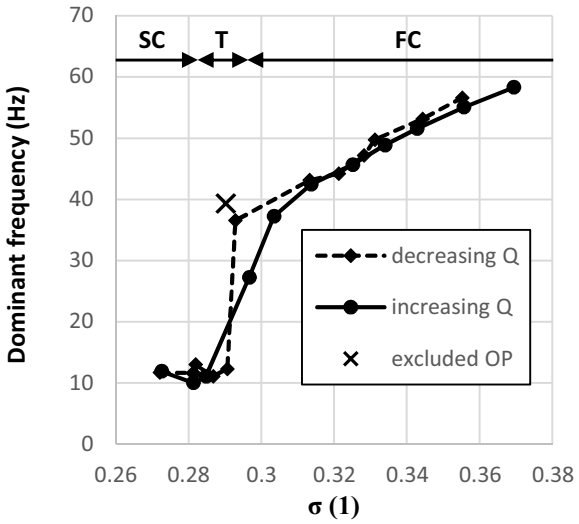

Fig. 22. Spectral analysis of the pressure pulsations recorded during the B1 measurement

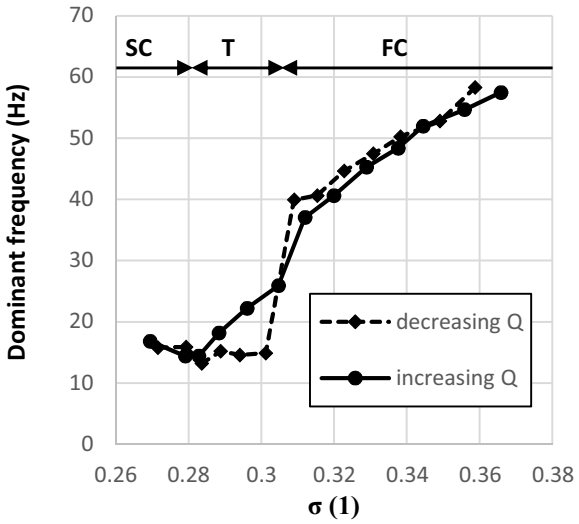

Fig. 23. Spectral analysis of the pressure pulsations recorded during the B2 measurement

As an additional information confirming the assumption that the neglecting of the temperature growth does not affect the obtained result significantly in case of measurement A, the change of the water temperature during the measurement B is depicted in the following figure. It can be seen that increase of the water temperature was approximately 1°C per experimental cycle (Figure 24).

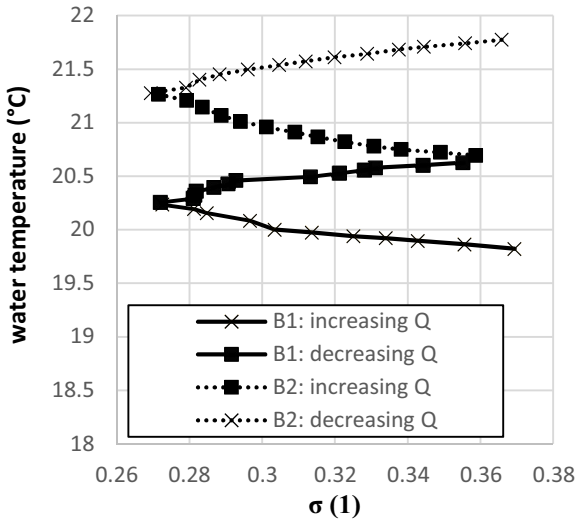

Fig. 24. Growth of the water temperature during the experimental cycles

Hydraulic losses have been evaluated in case of measurements B as it was mentioned above. The results are depicted in the following figures (25 and 26).
The results are fully comparable with each other from the direction of the discharge change as well as from the reproducibility point of view. It should be particularly emphasized that no significant difference between the hydraulic loss coefficient of corresponding cavitation number was observed depending on the direction of the discharge change.
Therefore, it can be stated that no significant signs of cavitation hysteresis have been observed during the evaluation of experiments. The only visible difference, which was observed and proved was the slightly earlier occurrence of the transition between cavitation regimes in case of increasing discharge. It has been possibly caused by larger amount of residual bubbles, attached to the walls of nozzle, which can play a role of cavitation nuclei.

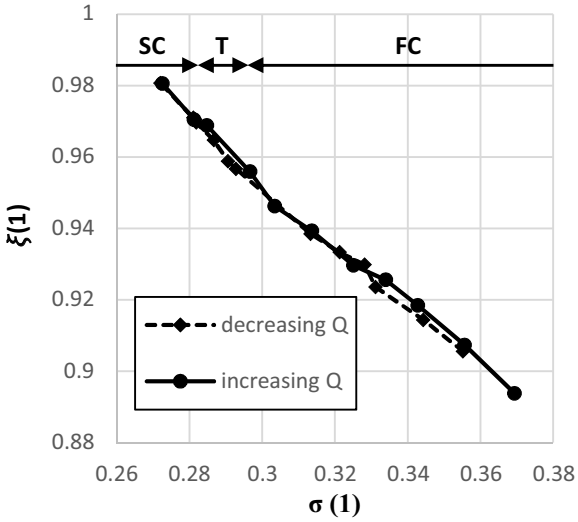

Fig. 25. Hydraulic losses evaluated using the results B1measurement

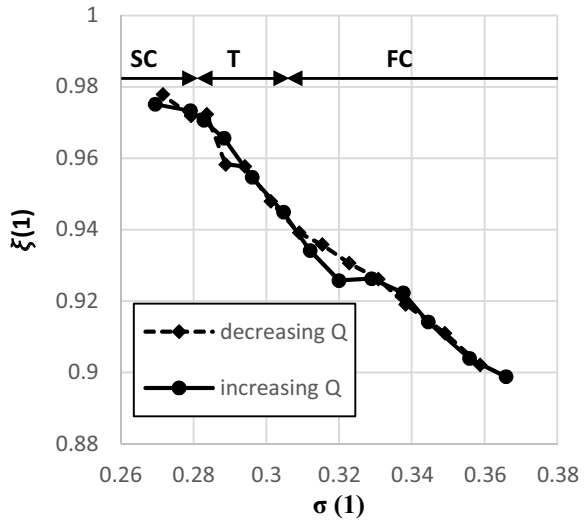

Fig. 26. Hydraulic losses evaluated using the results of B2 measurement

6 Future outlook

The presented methodology of the HS analysis will be applied for the investigation of the cavitation within the same Venturi tube, affected by the presence of the upstream swirl generator.

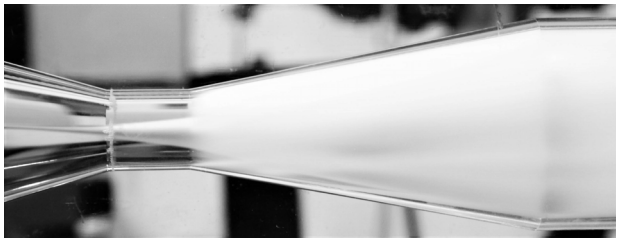

Fig. 27. Cavitation affected by the vortex within the Venturi tube (test measurement)

7 Conclusions

Dynamics of the cavitating flow within Venturi tube considering different gradient of the discharge change has been studied in the presented contribution. Above that, the hydraulic losses have been evaluated. Using these results, the possible occurrence of the hysteresis during the transition between fully developed cavitation and supercavitation has been discussed.

For the purpose of the investigation two experimental measurements have been carried out.

During the measurement A, the HS camera has been utilized to provide overall view of cavitation phenomenon as well as source data for the further image analysis.

Two different methods of the image analysis have been utilized: Spectral analysis of the pixel intensity fluctuations with semi-automated choice of the source pixel and proper orthogonal decomposition of the records. The choice of the source pixel for the purpose of FFT has been based on the maximum value of pixel intensity root mean square. This criterion provides quite robust as well as objective results.

The POD has been described in details. The provided results are in good agreement with the FFT analysis, but the additional information resulting from the decomposition are also useful. Distinguishing of the cavitation regimes using the analysis of the POD modes significance distribution was possible in this particular example of cavitating flow analysis.

Above that it was possible to state, that in case of the increasing discharge cycle the curve of the cumulative significance corresponding to the transition was significantly closer to the supercavitation curve compared to the results of decreasing discharge cycle analysis. This means that more significance (or information about the captured instabilities) is cumulated in the higher POD modes, e.g. the flow is more fluctuating.

It corresponds to the observation that the records of increasing discharge cycle contained larger amount of small bubbles. This results also suggests, that the transition to supercavitation occurred slightly earlier in case of increasing discharge cycle.

At the end of the measurement A, the results of the image analysis methods have been correlated together and with the results of the pressure fluctuations spectral analysis with a good degree of agreement.

To provide information about the hydraulic losses and to prove that the temperature growth during the measurement A can be neglected, the measurement B has been carried out. This measurement has been done twice to partially prove results reproducibility.

It is possible to state, that it is possible to reproduce the results of experiments, based on the analysis of the repeated measurements.

Approximate increase of temperature was 1°C per cycle of the measurement. Therefore, the temperature increase neglect should not significantly affect the results of the measurement A.

During the measurement B the hydraulic losses as well as spectral analysis of the pressure pulsation has been done. No significant difference has been observed from the hydraulic losses point of view. On the other hand, it has been clearly depicted that in case of the spectral analysis one can see that the transition regime began earlier in case of the increasing discharge while in case of the decreasing discharge cycle the cavitation regime change was more abrupt. This result is in good agreement with the conclusions of measurement A.

The final conclusion of the investigation is that no significant presence of the cavitation hysteresis has been observed or proved from the dominant frequencies related to the cavitation fluctuations point of view. Neither the analysis of the hydraulic losses has not proved any significant difference caused by the direction of the discharge change. The only captured and proved difference is the earlier occurrence of the transition between regimes in case of increasing discharge.

The presented methodology of the HS records analysis will be utilized in the further investigation of the cavitation within the Venturi tube.

References

1. P. Dörfler, M. Sick M., A. Coutu, *Flow-induced pulsation and vibration in hydroelectric machinery: engineer's guidebook for planning, design and troubleshooting.* London: Springer, ISBN 978-1-4471-4251-5, (2013)
2. D. Jančura, P. Mikula, B. Maršálek, P. Rudolf, F. Pochýly, *Selective method for cyanobacterial bloom removal: hydraulic jet cavitation experience,* Aquaculture International, vol.: **22** Issue: **2** Pages: 509-521, DOI: 10.1007/s10499-013-9660-7, (2014)
3. P. Rudolf., M. Hudec, P. Zubík., D. Štefan, *Experimental measurement and numerical modeling of cavitating flow in converging-diverging nozzle.* EPJ Web of Conferences **25**, DOI: 10.1051/epjconf/20122501081, (2012)
4. J. Kozák, P. Rudolf, D. Štefan, M. Hudec, M. Gríger, *Analysis Of Pressure Pulsations Of Cavitating Flow In Converging-Diverging Nozzle*. 6th IAHR International Meeting of the Workgroup on Cavitation and Dynamic Problems in Hydraulic Machinery and Systems, (2015)
5. J. Jablonská, M. Kozubková, D. Himr, M Weisz, *Methods Of Experimental Investigation Of Cavitation In A Convergent - Divergent Nozzle Of Rectangular Cross Section*. Measurement Science Review, vol.: **16**, DOI: 10.1515/msr-2016-0024, (2016)
6. Engineering toolbox [online], cited 2016-07-20, <http://www.engineeringtoolbox.com/water-vapor-saturation-pressure-air -d_689.html>,(2016)
7. Cooley, James W., and John W. Tukey. 1965. *An Algorithm For The Machine Calculation Of Complex Fourier Series*. In *Mathematics Of Computation*, vol. **19**, issue **90**, DOI:10.1090/S0025-5718-1965-0178586-1 (1965)
8. M. Sedlář, M. Komárek, P. Rudolf, J. Kozák, R. Huzlík, *Numerical and experimental research on unsteady cavitating flow around NACA 2412 hydrofoil*. IOP Conference Series: Materials Science and Engineering, vol. **72**, issue **2**, DOI: 10.1088/1757-899X/72/2/022014, (2015)
9. G. Berkooz, P. Holmes, J. Lumley, *The proper orthogonal decomposition in the analysis of turbulent flows,* Annual Rev. of Fluid Mechanics vol. **25**(1), Pages: 539-575, (1993)
10. D. Stefan,P. Rudolf, *Proper Orthogonal Decomposition of Pressure Fields in a Draft Tube Cone of the Francis (Tokke) Turbine Model*, Journal of Physics: Conference Series, vol. **579**, DOI : 10.1088/1742-6596/579/1/012002, (2015)
11. P. Rudolf, D. Štefan, M. Sedlář, J. Kozák, V. Habán, R. Huzlík, *Spatio-temporal description of the cavitating flow behavior around NACA 2412 hydrofoil*, Journal of Physics: Conference Series, vol. **656**, DOI: 10.1088/1742-6596/656/1/012168, (2015)
12. P. Tomov, A. Danlos, S. Khelladi, F. Ravelet, C. Sarraf, F. Bakir, *POD study of aerated cavitation in a venturi nozzle*, Journal of Physics: Conference Series, vol. **656**, DOI : 10.1088/1742-6596/656/1/012171, (2015)
13. A. Danlos, F. Ravelet, O. Coutier-Delgosha, F. Bakir, C. Sarraf, F. Bakir, *Cavitation regime detection through Proper Orthogonal Decomposition:Dynamics analysis of the sheet cavity on a grooved convergent–divergent nozzle*, International Journal of Heat and Fluid Flow, vol. **47**, DOI : 10.1016/j.ijheatfluidflow.2014.02.001, (2014)

Acknowledgement

Czech Science Foundation is gratefully acknowledged for support of this research under project No 16-18316S „Principles and mechanisms causing microorganism elimination by hydrodynamic cavitation“.